Dalton Transactions

Accepted Manuscript

ROYAL SOCIETY OF CHEMISTRY

www.rsc.org/dalton

Two water-bridged cobalt(II) chains with isomeric naphthoate spacers: from metamagnetic to single-chain magnetic behaviour

Zhong-Yi Liu,[a] Yan-Fei Xia,[a] En-Cui Yang,[a,*] and Xiao-Jun Zhao [a,b*]

To *Dalton Trans* (Article)

[a] *College of Chemistry, Key Laboratory of Inorganic-Organic Hybrid Functional Material Chemistry, Ministry of Education, Tianjin Key Laboratory of Structure and Performance for Functional Molecules, Tianjin Normal University, Tianjin 300387, P. R. China.* E-mail: encui_yang@163.com, *xiaojun_zhao15@163.com*; *Fax:+86-22-23766556*

[b] *Collaborative Innovation Center of Chemical Science and Engineering (Tianjin), Tianjin 300071, China*

† Electronic supplementary information (ESI) available: TG curves, PXRD patterns, magnetic and heat capacity results for **1**–**2** and X-ray crystallographic file in CIF format for **1**. CCDC 994391 for **1** and 623817 for **2**. For ESI and crystallographic data in CIF or other electronic format see DOI:10.1039/

Crystal structures and magnetic behaviours of two water-bridged one-dimensional (1D) cobalt(II) chains with different isomeric naphthoate (na^-) terminals, $[Co(H_2O)_3(2\text{-}na)_2]_n$ (**1**) and $\{[Co(H_2O)_3(1\text{-}na)_2]\cdot 2H_2O\}_n$ (**2**), were reported to investigate the effect of interchain distance on the magnetic properties. Complex **1** with *trans*-2-na^- blocks and dense interchain separation exhibits a metamagnetic transition from antiferromagnetic ordering to a saturated paramagnetic phase. By contrast, complex **2** possessing *cis*-arranged 1-na^- spacers and well interchain isolation behaves as unusual single-chain magnetic behavior under zero dc field. Thus, completely different interchain packing by isomeric naphthoate ligand governs the ratio between intra- and interchain magnetic interaction and further results in different magnetic phenomena, which provide significant magnetostructural information on the 1D magnetic systems.

Introduction

One-dimensional (1D) magnetic chains constructed from different spin carriers and short organic mediators have always evoked great interest due to their simple structures for better understanding the fundamental magnetostructural relationships, as well as their promising applications in high-density information storage and molecular spintronics.[1–9] Up to date, lots of 1D homo- or heterospin systems have been successively generated by combinations of transition/rare-earth metal ions with variable magnetic nature and organic radicals,[6] azide,[10] oximate,[11] carboxylate,[12] cyanide,[13] thiocyanate[14] and so on. These resulting samples have exhibited diverse long-range ordering (LRO) (ferro-, antiferro-, ferri-, as well as metamagnets) and/or single-chain magnetic (SCM) behaviours, which significantly rely on the anisotropy of the spin carrier, the types and magnitudes of the intrachain exchange couplings, as well as the ratios of intra- and interchain magnetic interactions. Apparently, for a given chain constructed from the same spin carrier and short magnetic mediator, the interplay of intra- and interchain magnetic interactions play important roles for the resulting magnetic phenomena.[15] A suitable ratio of intra- to interchain magnetic interaction can induce the co-existence of LRO and SCM and can even switch the LRO to SCM behavior.[5] Thus, some effective methods to increase the interchain distance and minimize the interchain magnetic interaction have been proposed to obtain high performance SCMs. These commonly used approaches usually include introducing lattice solvent molecules as magnetic separators,[16] controlling interchain hydrogen-bonding interactions,[17] selecting longer and multitopic organic spacers,[18] as well as implanting bulky conjugate porphyrin bridges.[19] However, the intrinsic magnetostructural correlations between the LRO and SCM behaviour remain incomplete and challenging because of the inherent difficulties in controlling the packing of substructures.[20–22]

Possessing strongly anisotropic Co^{II} spin and short single-atom O bridge, water extended cobalt(II) chain

can be considered as a simple model to understand the complicated magnetostructural relationships. Up to date, at least ten –Co^{II}–H_2O–Co^{II}– chains have been reported (CSD, May 2015 release)[23] by varying the different terminal ligands,[24–28] and only four of them have been magnetically investigated to exhibit spin-canted antiferromagnetism and SCM behavior.[24–27] Herein, as part of ongoing investigations along this line, a new single water-bridged 1D cobalt(II) chain with *trans*-2-naphthoate (2-na^-) spacers, $[Co(H_2O)_3(2\text{-na})_2]_n$ (**1**), was successfully obtained and magnetically characterized. More interestingly, **1** is structurally comparable to a analogue with a pair of *cis*-orientated 1-naphthoate (1-na^-) terminus, $\{[Co(H_2O)_3(1\text{-na})_2]\cdot 2H_2O\}_n$ (**2**). In fact, the crystal structure and fluorescent property of **2** was previously reported by our group.[29] Now, we are interested in the magnetic behavior of **2** and focus specially on the effect of interchain packing patterns on the resulting magnetic phenomena. In this context, crystal structures and magnetic properties of these twin complexes were presented and the effect of isomeric naphthoate terminus on the exchange coupling and magnetic dynamics were discussed in more detail.

Experimental

Materials and instruments

All initial chemicals were commercially purchased (2-Hna was from Acros and other analytical-grade reagents were from Tianjin Chemical Reagent Factory) and used as received without further purification. Doubly deionized water was used for the conventional synthesis. Elemental analyses for C and H were carried out with a CE–440 (Leeman–Labs) analyzer. Fourier transform (FT) IR spectra (KBr pellets) were taken on an Avatar–370 (Nicolet) spectrometer in the range 4000–400 cm^{-1}. Thermogravimetric analysis (TGA) experiment was performed on a Shimadzu simultaneous DTG–60A compositional analysis instrument from room temperature to 800 ºC under N_2 atmosphere at a heating rate of 5 ºC min^{-1}. Powder X–ray diffraction (PXRD) patterns were obtained from a Bruker D8 ADVANCE diffractometer at 40 kV

and 40 mA for Cu Kα radiation (λ = 1.5406 Å), with a scan speed of 0.1 sec/step and a step size of 0.01º in 2*θ*. The simulated PXRD pattern was calculated using single-crystal X-ray diffraction data and processed by the free Mercury v1.4 program provided by the Cambridge Crystallographic Data Center. Magnetic susceptibilities were acquired on a Quantum Design (SQUID) magnetometer MPMS-XL-7 with crystalline samples. The diamagnetism corrections including the sample holder and the constituents were done with the Pascal's tables. Heat capacity measurements were performed with the PPMS-9 Quantum Design apparatus equipped with a heat capacity module and He^3 components, in which the signals from the mount and grease used to hold the sample were also eliminated.

Synthesis of $[Co(H_2O)_3(2\text{-na})_2]_n$ (1). 2-Hna (34.5 mg, 0.2 mmol) was dissolved in methanol solution (4.0 mL), and the initial pH value of the mixture was adjusted to 6 with an aqueous NaOH solution (M = 0.25 mol L^{-1}). Then, an aqueous solution (6.0 mL) of $Co(CH_3COO)_2{\cdot}4H_2O$ (74.7 mg, 0.3 mmol) was added dropwise to the above mixture with constant stirring. The resulting mixture was further stirred for about one hour and filtered. Pink block-shaped crystals of **1** suitable for X-ray analysis were generated by slow evaporation of the filtrate within one week (Yield: 33.3% based on 2-Hna). Anal. Calcd for $C_{22}H_{20}O_7Co$: C, 58.03; H, 4.43%. Found: C, 58.07; H, 4.40%. IR (KBr, cm^{-1}): 3341 (br), 3053 (w), 1599 (s), 1524 (s), 1419 (s), 1360 (s), 1241 (m), 1206 (m), 1140 (w), 795 (m), 782 (m), 734 (w), 636 (w), 599 (w), 488 (w), 476 (w).

Synthesis of $\{[Co(H_2O)_3(1\text{-na})_2]\cdot 2H_2O\}_n$ (2). Complex **2** was synthesized in an aqueous solution according the procedures reported by our group (Yield: 60.2% based on 1-Hna).[29] Anal. Calcd for $C_{44}H_{48}O_{18}Co_2$: C, 53.78; H, 4.92%. Found: C, 53.67; H, 5.00%. The crystal structure of **2** was also confirmed by single-crystal X-ray determinations.

X-Ray data collection and structure determination

Diffraction intensity of **1** was collected on a Bruker APEX-II CCD diffractometer equipped with graphite-monochromated Mo *K*α radiation with a radiation wavelength of 0.71073 Å by using the φ–ω scan technique at 296 K. There was no evidence of crystal decay during data collection. Semiempirical multi-scan absorption corrections were applied by *SADABS*[30] and the program *SAINT*[31] was used for integration of the diffraction profiles. The structures were solved by direct methods and refined with the full-matrix least-squares technique using the *SHELXS-97* and *SHELXL-97* programs.[32] Non-H atom was located by difference Fourier maps and subjected to anisotropic refinement. H atom was added according to theoretical models. The crystallographic data, selected bond lengths and angles, as well as the hydrogen-bonding parameters for **1** were given in Tables 1 ~ 3, respectively.

/insert Table 1/

Results and discussion

Syntheses and conventional characterizations

The twin complexes with isomeric naphthoate ligands were successfully prepared by room-temperature evaporation method in satisfactory yields. In the IR spectrum of **1** (Fig. S1), a broad and strong band centered at 3341 cm^{-1} indicated the presence of water molecule. An absence of a strong absorption at *ca* 1675 cm^{-1} confirmed the deprotonation of 2-Hna ligand.[33] The asymmetric (ν_s) and symmetric (ν_{as}) vibrations for the carboxylate group of 2-na^- anion were observed at 1599, 1524 and 1413, 1355 cm^{-1}, and their separation ($\Delta\nu = \nu_s - \nu_{as}$ = 111 cm^{-1}) is dramatically different from that of **1**.[29] The obvious difference on the characteristic vibrations of the carboxylate group should be ascribed to more intramolecular hydrogen-bonding interactions of **2** than **1**, rather than the binding mode of the carboxylate moiety to Co^{II} ion. TGA measurement revealed (Fig. S2) that three coordinated water molecules of **1** (4.38 mg, 100%) were released between 99 and 163ºC (obsd. 0.51 mg, 11.6%; calcd. 0.52 mg, 11.9%). The 2-na^- anion was

decomposed between 303 and 800 ºC, leaving CoO as final product (obsd. 0.69 mg, 15.7%; calcd. 0.72 mg, 16.5%). The phase purity and the structural consistency of bulky products of **1** and **2** were further identified by the consistency of the calculated and experimental PXRD patterns (Fig. S3).

Crystal structures of 1–2

$[Co(H_2O)_3(2\text{-na})_2]_n$ (1). Complex **1** crystallizes in the monoclinic *P*2/*c* space group (Table 1), exhibiting a scarcely observed water extended 1D chain with a pair of unidentate 2-na$^-$ anions as terminal spacers. The asymmetric unit of **1** consists of half a Co^{II} ion located at an inversion center, one monodeprotonated 2-na$^-$ anion, one terminal aqua ligand, as well as half a bridging water molecule. As shown in Fig. 1, the centrosymmetric Co^{II} atom in **1** adopts axially elongated octahedral coordination geometry with four water molecules located in the *cis*-positions and two unidentate carboxylate O donors from two separate 2-na$^-$ anions in a *trans*-alignment. The axial Co–$O_{bridging\ aqua}$ bond lengths are *ca* 0.2 Å longer than those of Co–$O_{terminal\ aqua/carboxylate}$ in the equatorial plane (Table 2).

/*insert Fig. 1 and Table 2*/

Adjacent Co^{II} octahedra are periodically propagated by bridging water molecules, leading to a bent 1D chain running along the crystallographic *c*-axis (Fig. 1 top). The intrachain intermetallic distance and the bridging angle of ∠Co–O_{aqua}–Co are 4.0073(1) Å and 127.950(3)°, favorable for mediating antiferromagnetic interactions.[34] Furthermore, the individual chains of **1** interact with each other by interchain O_{aqua}–H···$O_{carboxylate}$ (Table 3) and C–H···π interactions, leading to a two-dimensional (2D) supramolecular layer with the nearest interchain intermetallic separation of 6.3428(13) Å (Fig. 2 top).

/*insert Fig. 2 and Table 3*/

$\{[Co(H_2O)_3(1\text{-na})_2]\cdot 2H_2O\}_n$ (2). Crystal structure **2** was previously reported, also featuring a 1D chain with adjacent octahedral Co^{II} spins extended by bridging water molecules. For better understanding the

structure-dependent magnetic behaviour, the crystal structure of **2** and its significant difference from that of **1** were presented herein. Actually, three vital differences between the twin complexes can be summarized through careful comparisons of their crystal structures. Firstly, **2** crystallizes from the monoclinic $P2_1/n$ space group, in which two symmetry-related 1-na$^-$ ligands are in the *cis* positions of the octahedral Co^{II} ion (Fig. 1 bottom). Secondly, the intrachain intermetallic distance and the bridging angle of ∠Co–O_{aqua}–Co are 4.081(2) Å and 131.783(13)°, which are moderately different from those of **1**. Finally, just due to the *cis*-arrangement of the two 1-na$^-$ anions, the adjacent chains of **2** are well separated by interchain C-H···π interactions, generating a non-covalent 2D layer with the nearest interchain intermetallic distance of 12.7436(6) Å (Fig. 2 bottom). Two lattice water molecules are hydrogen-bonded to the separate 1D chain (Fig. 2 bottom, Fig. S4 and Table S1), enhancing the robustness of the individual chain. It should be noted that the interchain separation of **2** is almost double of **1**, meaning that the interchain packing of **2** is much loose than that of **1**. The dramatically different interchain isolations of the two samples are expected to direct different interchain magnetic interactions, providing a good chance to explore their magnetostructural relationships.

Magnetic properties

/insert Fig. 3/

Variable-temperature direct current (dc) magnetic susceptibilities were measured on the freshly prepared, crystalline samples of **1** and **2** under an applied field of 1 kOe. As shown in Fig. 3, the $\chi_M T$ product for each Co^{II} ion of **1** is 3.11 cm^3 mol^{-1} K at 300 K, which is common for one high-spin Co^{II} octahedron due to the large orbital contribution.[34] The $\chi_M T$ value of **1** decreases monotonously with the decreasing temperature and reaches a value of 0.09 cm^3 mol^{-1} K at 2.0 K. Fitting the magnetic data of **1** to the Curie–Weiss law above 12.0 K gives Curie constant C = 3.50 cm^3 mol^{-1} K and Weiss constant θ = –42.11 K (Fig. S5),

indicating that dominant antiferromagnetic coupling occurs between the nearest neighbors of the spin carriers and spin-orbit coupling effect of the octahedral Co^{II} ion. To quantitatively evaluate the intra- and interchain antiferromagnetic interactions, the molar susceptibility of **1** was treated by a Fisher 1D chain model with a molecular-field approximation to describe the interchain magnetic couplings (zJ'),[35] the fitting equations are as following:

$$\chi_{chain} = [Ng^2\beta^2S(S+1)/(3kT)][(1+u)/(1-u)] \qquad (1)$$

where $u = \coth[JS(S+1)/kT]-kT/[JS(S+1)]$

$$\chi_M = \chi_{chain} / [1-(zJ'\chi_{chain}/Ng^2\beta^2)] \qquad (2)$$

The best least-squares fitting of the molar susceptibility of **1** above 70.0 K leads to g = 2.62(2), J = –3.44(0) cm^{-1}, zJ' = –0.71(3) cm^{-1}, and R = 3.1×10^{-4} (R is the agreement factor defined as $R = \Sigma[(\chi_MT)_{obsd}-(\chi_MT)_{calcd}]^2/\Sigma[(\chi_MT)_{obsd}]^2$). The obtained coupling constants suggest that the superexchange interactions through the single water bridge and O–H···O hydrogen-bonding are both antiferromagnetic but nonequivalent, in which the interchain coupling strength is almost one fifth of the intrachain one ($J_{intrachain}/J_{interchain}$ = 4.8). Notably, the χ_M–T curves of **1** display a sharp maximum at ca. 4.5 K under an applied field of 4, 6 and 8 kOe (Fig. 3), implying an antiferromagnetic ordering at low fields. The Néel temperature (T_N) is estimated to be 4.1 K by temperature-dependent alternate current (ac) magnetic susceptibility (Fig. S6). Interestingly, the maximum disappears once the field is beyond 12 kOe, revealing a field-induced metamagnetic transition from an antiferromagnetic ordering to a saturated paramagnetic phase.

The metamagnetism of **1** can also be confirmed by the sigmoid-shaped isothermal magnetization curve measured at 2.0 K (Fig. 4), in which the critical field is estimated to be 7.0 kOe by dM/dH at 2.0 K (Fig. S7). The magnetization of **1** at 50 kOe (0.65 $N\beta$) is far from the saturation value for one octahedral Co^{II} ion

(2.4–3.0 $N\beta$), indicating the presence of spin-canting. The spin-canted structure is in accordance with the structure of **1** where the Jahn-Teller axes of two adjacent Co^{II} octahedra are not parallel to each other but form an angle (γ) of 52.941°. Extrapolating the high-field linear part of the magnetization curve to zero field gives the remnant magnetization of 0.17 $N\beta$ (Mr). Thus, the canting angle (φ) of **1** is 2.5° estimated by the equation $\varphi = \tan^{-1}(M_r/M_s)$ ($M_s = gS = 3.93\ N\beta$, $S = 3/2$, $g = 2.62$).[36–37] The canting angle is smaller than γ because the antiferromagnetic interactions tend to align the spin vectors in an antiparallel mode. The hysteresis loop of **1** measured at 2.0 K exhibits no obvious opening, consistent with the strong antiferromagnetic (AF) phase of **1** under low fields (Fig. 4 inset).

To fully understand the metamagnetic behaviour of **1**, field-dependent magnetizations were collected at different temperatures (2.0 – 4.0 K). By coming the maxima observed in the dM/dH versus H and χ_M versus T data (Fig. S7), an magnetic phase diagram (H, T) of **1** was constructed, as shown in Fig. 5. Notably, the phase-transition curve extrapolates to $T = 0$ K at approximately $H_c(0) = 7.4$ kOe and vanishes at $T_N = 4.1$ K. The phase diagram of **1** is typical for an antiferromagnet with a metamagnetic behaviour.[38–39] The $H_c(T)$ line corresponds to a canted AF/paramagnetic phase transition that occurs when the magnetic field is applied along the easy direction of the magnetization. Low T_N is consistent with the presence of a very weak interchain AF interaction estimated by the critical field. Heat capacity measurement of **1** was also carried out at low temperature under zero dc field (Fig. S8), and an obvious peak at 4.0 K confirms the phase transition of **1** from an antiferromagnetic ordering to a saturated paramagnetic phase.

/*insert Fig. 4 and Fig. 5*/

To investigate the magnetic dynamics, alternate current (ac) magnetic susceptibilities of **1** were measured under zero dc field over the frequencies of 10 to 1000 Hz with an oscillating 3.5 Oe ac field. As a result, both the χ' and χ'' components are frequency-independent, suggesting that no magnetic relaxation occurs in

the antiferromagnetic phase of **1** due to the relatively strong interchain interactions ($J_{intrachain}/J_{interchain}$ = 4.8). An obvious peak observed for the χ' component together with an negligible χ'' signals hint the antiferromagnetic ordering state with T_N = 4.1 K (Fig. S6).

The low-temperature susceptibility of **2** is much different from those of **1**, although the room-temperature $\chi_M T$ value (3.05 cm^3 mol^{-1} K) is comparable to that of **1**. Upon cooling, the $\chi_M T$ of **2** continuously decreases to 0.23 cm^3 mol^{-1} K at 3.5 K, then increases abruptly to a maximum of 0.28 cm^3 mol^{-1} K at 2.0 K (Fig. 3 right). The sudden increase of $\chi_M T$ at low temperature suggests an onset of a weak spontaneous magnetization state. The $\chi_M T$ curves of **2** are also field-dependent below 3.5 K, consistent with a canted antiferromagnetic behaviour. Fit the data above 40 K to the Curie-Weiss law gives C = 3.19 cm^3 mol^{-1} K and θ = –36.43 K (Fig. S5), also implying dominant antiferromagnetic interactions exist in the 1D chain of **2**. Furthermore, the same magnetic model for **1** is used to treat the magnetic exchange between Co^{II} ions of **2**, due to the analogous 1D magnetic chain with the same spin carrier. Above 70.0 K, the best fitted values are g = 2.61(5), J = –3.56(3) cm^{-1}, zJ' = 0.05(2) cm^{-1}, and $R = 6.3\times10^{-4}$. As expected, the intrachain magnetic coupling of **2** is comparable to that of **1**. Surprisingly, the interchain interaction expressed as zJ' of **2** is greatly decreased as compared with that of **1**, which is obviously due to the larger interchain distance of **2**. The ratio of intra- to interchain magnetic interaction in **2** amounts up to 71.2.

Field-dependent isothermal magnetization of **2** measured at 2.0 K (Fig. 4) displays an abrupt increase below 4.0 kOe and is followed by a linear increase between 4 and 50 kOe. The magnetization of **2** at 50 kOe (0.44 $N\beta$) is far below the expected saturation value (2.4–3.0 $N\beta$) for one Co^{II} ion, consistent with the canting-induced weak ferromagnetism of **2**.[36] Furthermore, field-dependent magnetizations of **2** at different temperatures (Fig. S9) were measured to confirm that complex **2** does not show metamagnetic behavior

entirely different from that of **1**. Due to the absence of the magnetic ordering, the canting angle of **2** can not be calculated.

/insert Fig. 7/

Much different from **1**, frequency-dependent ac susceptibility of **2** was clearly observed below 1.7 K under a zero dc field (Fig. 6). The intensity of the χ'' peak increases with decreasing frequency, which is consistent with an ideal SCM behavior.[40] The Mydosh parameter $\varphi = (\Delta T_p/T_p)/\Delta(\log f)$ (T_p is the peak temperature of χ') estimated from this dependence is 0.21, consistent with superparamagnets including SCM as reported for **2**.[3] The maximum of the peaks observed in the temperature dependent ac measurement were fitted to the Arrhenius law to give an effective energy barrier Δ_τ/k_B = 15.6 K and the pre-exponential factor $\tau_o = 5.8\times10^{-8}$ s (Fig. 6 inset), which is compared with an previously reported H_2O-bridged Co^{II} subchain confined in a 3D framework with a long organic connector to separate the interchain interactions.[24] The fitting of Cole–Cole plots of **2** in the range of 0.1–1000 Hz (Fig. S10) exhibit α = 0.14 at 1.4 K. The parameter α is a value between 0 and 1, which gauges the width of the relaxation time distribution.[41] α = 0 describes a single relaxation process as expected for ideal SCM, and α = 0.14 means a relative narrow distribution of the relaxation time, which is comparable to previously reported SCMs. Hysteresis loops respectively measured at 2.0 and 1.0 K gave negligible coercive field and remnant magnetization, suggesting that the relaxations of **2** above 1.0 K are too fast (Fig. 4 insert).

To further examine the 1D nature and the presence of significant magnetic anisotropy of **2**, the linear dependence of the $\ln(\chi'_M T)$ versus $1/T$ was plotted, where χ' is the in-phase ac susceptibility measured at 1 Hz under zero dc field. As show in Fig. 7, a linear fitting of these data between 1.7 and 3.0 K to the expression $\chi_M T \approx C_{eff}(\Delta_\xi/k_B T)$ (C_{eff} is the effective Curie constant and Δ_ξ is the energy to create a domain wall in the chain) leads to a positive slope of 4.12 K, which means that the correlation energy (Δ_ξ/k) is 4.12

K.[42] Because the magnetic relaxation of **2** occurs below 1.7 K (T^{-1} = 0.59), the 1D chain nature of **2** locates in the finite-size regime and the equation $\Delta_\tau = \Delta_\xi + \Delta_A$ can be used to estimate the anisotropy energy gap (Δ_A).[3] Based on the obtaining Δ_τ and Δ_ξ parameters, the Δ_A/k_B of **2** is 11.48 K, which is satisfied with the Glauber criterion ($\Delta_A > \Delta_\xi$) and in accordance with the Ising nature.[3, 43] Additionally, temperature-dependent heat capacity (C_p) experiments of **2** were measured at low temperature region under zero and 5 kOe dc fields, respectively (Fig. S8). The absence of any obvious peaks in C_p–T curves further confirms the SCM nature of **2**, eliminating the transition and/or co-existence of two different magnetic phases. In summary, complex **2** with two *cis*-arranged 1-na$^-$ spacers and well interchain isolation exhibits SCM behavior at low temperature, which is dramatically different from the metamagnetic nature of **1** with *trans*-aligned 2-na$^-$ ligand and close interchain separation.

Conclusion

In conclusion, two water-bridged 1D cobalt(II) chains with isomeric naphthoate terminus were obtained and exhibit metamagnetic and SCM behaviours resulting from the interplay between intra- and inter-chain magnetic interactions. These interesting results indicate that the terminal isomers can influence the interchain magnetic interactions through regulating the packing mode of 1D chains.

Acknowledgements

This present work was financially supported by the National Natural Science Foundation of China (Grants 21171129, 21173157, 21371134, and 21303121), the Program for Innovative Research Team in University of Tianjin (TD12-5038) and Tianjin Municipal Education Commission (2012ZD02), which are gratefully acknowledged.

References

1 L. Öhrström and K. Larsson, *Molecule-Based Materials: The structural Network Approach*, Elsevier: Amsterdam, 2005.

2 H.-L. Sun, Z.-M. Wang and S. Gao, *Coord. Chem. Rev*., 2010, **9–10**, 1081.

3 L. Bogani, A. Vindigni, R. Sessoli and D. Gatteschi, *J. Mater. Chem.*, 2008, **18**, 4733.

4 H. Miyasaka, M. Julve, M. Yamashita and R. Clérac, *Inorg. Chem.*, 2009, **48**, 3420.

5 W.-X. Zhang, R. Ishikawa, B. Breedlove and M. Yamashita, *RSC Adv*., 2013, **3**, 3772.

6 (*a*) A. Caneschi, D. Gatteschi, N. Lalioti, C. Sangregorio, R. Sessoli, G. Venturi, A. Vindigni, A. Rettori, M. G. Pini and M. A. Novak, *Angew. Chem. Int. Ed*., 2001, **40**, 1760; (*b*) K. Bernot, J. Luzon, R. Sessoli, A. Vindigni, J. Thion, S. Richeter, D. Leclercq, J. Larionova and A. Lee, *J. Am. Chem. Soc.*, 2008, **130**, 1619.

7 T.-F. Liu, D. Fu, S. Gao, Y.-Z. Zhang, H.-L. Sun, G. Su and Y.-J. Liu, *J. Am. Chem. Soc.*, 2003, **125**, 13976.

8 H.-B. Zhou, J. Wang. H.-S. Wang, Y.-L. Xu, X.-J. Song, Y. Song and X.-Z. You, *Inorg. Chem*., 2011, **50**, 6868.

9 Y. Oka, K. Inoue, H. Kumagai and M. Kurmoo, *Inorg. Chem*., 2013, **52**, 2142.

10 Y.-F. Zeng, X. Hu, F.-C. Liu and X.-H. Bu, *Chem. Soc. Rev*., 2009, **38**, 469.

11 C.-I. Yang, S.-P. Huang, G.-H. Lee, M. Nakano and H.-L. Tsai, *Inorg. Chem*., 2010, **49**, 7617.

12 Y. Li, J.-W. Yu, Z.-Y. Liu, E.-C. Yang and X.-J. Zhao, *Inorg. Chem*., 2015, **54**, 153.

13 S. Wang, J.-L. Zuo, S. Gao, Y. Song, H.-C. Zhou, Y.-Z. Zhang and X.-Z. You, *J. Am. Chem. Soc*., 2004, **126**, 8900.

14 (*a*) J. Boeckmann and C. Näther, *Chem. Commun*., 2011, **47**, 7104; (*b*) S. Wöhlert, J. Boeckmann, M. Wriedt and C. Näther, *Angew. Chem. Int. Ed*., 2011, **50**, 6920; (*c*) S. Wöhlert, T. Fic, Z. Tomkowicz, S. G. Ebbinghaus, M. Rams, W. Haase and C. Näther, *Inorg. Chem*., 2013, **52**, 12947; (*d*) S. Wöhlert, Z. Tomkowicz, M. Rams, S. G. Ebbinghaus, L. Fink. M. U. Schmidt and C. Näther, *Inorg. Chem*., 2014, **53**, 8298.

15 L. M. Toma, C. Ruiz-Pérez, J. Pasán, W. Wernsdorfer, F. Lloret and M. Julve, *J. Am. Chem. Soc*., 2012, **134**, 15265.

16 H. Miyasaka, K. Takayama, A. Saitoh, S. Furukawa, M. Yamashita and R. Clérac, *Chem. Eur. J*., 2010, **16**, 3656.

17 W.-X. Zhang, T. Shiga, H. Miyasaka and M. Yamashita, *J. Am. Chem. Soc*., 2012, **134**, 6908.

18 W. Ouellette, A. V. Prosvirin, K. Whitenackm, K. R. Dunbar and J. Zubieta, *Angew. Chem. Int. Ed*., 2009, **48**, 2140.

19 X. Chen, S.-Q. Wu, A.-L. Cui and H.-Z. Kou, *Chem. Commun*., 2014, **50**, 2120.

20 (*a*) L. Bogani, C. Sangregorio, R. Sessoli and D. Gatteschi, *Angew. Chem. Int. Ed*., 2005, **44**, 5817; (*b*) C. Benelli, A. Caneschi, D. Gatteschi and R. Sessoli, *Adv. Mater*., 1992, **4**, 504.

21 C.-M. Liu, D.-Q. Zhang and D.-B. Zhu, *Inorg. Chem*., 2009, **48**, 4980.

22 M. Yuan, F. Zhao, W. Zhang, Z.-M. Wang and S. Gao, *Inorg. Chem*., 2007, **46**, 11235.

23 F. H. Allen, *Acta Crystallogr., Sect. B: Struct. Sci*., 2002, **58**, 380.

24 X.-Z. Ma, Z.-J. Zhang, W. Shi, L.-L. Li, J.-Y. Zou and P. Cheng, *Chem. Commun*., 2014, **50**, 6340.

25 W.-H. Yan, S.-S. Bao, J. Huang, M. Ren, X.-L. Sheng, Z.-S. Cai, C.-S. Lu, Q.-J. Meng and L.-M. Zheng, *Dalton Trans.*, 2013, **42**, 8241.

26 D. Mikloš, J. Jašková, P. Segl'a, M. Korabik, J. Mrozinski, R. Sillanpää, M. Mikuriya and M. Melník, *Inorg. Chim Acta*, 2006, **359**, 4386.

27 H.-T. Xu and Z.-L. Xu, *Microporous Mesoporous Mater*., 2012, **157**, 33.

28 (*a*) Y.-Q. Zheng, J.-L. Lin, A.-Y. Pan, *Z. Anorg. Allg. Chem*., 2000, **626**, 1718; (*b*) T. Glowiak, H. Kozlowski, L. S. Erre, B. Gulinati, G. Micera, A. Pozzi and S. Bruni, *J. Coord. Chem*., 1992, **25**, 75; (*c*)

D. Miklos, J. Jaskova, P. Segla, J. Miklovic, V. Mrazova, B. Kalinakova, D. Hudecova, R. Sillanpaa, T. Lis and M. Melnik, *Monogr. Ser. Int. Conf. Coord. Chem*., 2005, **7**, 201; (*d*) H.-T. Xu and Z.-L. Xu, *Microporous Mesoporous Mater*., 2012, **157**, 33; (*e*) L. S. Erre, G. Micera, F. Cariati, G. Ciani, A. Sironi, H. Kozlowski and J. Baranowski, *J. Chem. Soc., Dalton Trans*., 1988, 363.

29 E.-C. Yang, P.-X. Dai, X.-G. Wang and X.-J. Zhao, *Transition Met. Chem*., 2007, **32**, 228.

30 G. M. Sheldrick, *SADABS*, University of Göttingen, Göttingen: Germany, 1996.

31 Bruker AXS, SAINT s*oftware Reference Manual*, WI, 1998.

32 (*a*) G. M. Sheldrick, *SHELXL-97, Program for X-ray Crystal Structure Refinement*; University of Göttingen: Göttingen, Germany, 1997; (*b*) G. M. Sheldrick, *SHELXS-97, Program for X-ray Crystal Structure Sloution*; University of Göttingen: Göttingen, Germany, 1997.

33 K. Nakamoto, *Infrared and Roman Spectra of Inorganic and Coordination Compounds*, Wiley: New York, 1986.

34 M. Kurmoo, *Chem. Soc. Rev*., 2009, **38**, 1353.

35 M. E. Fisher, *Am. J. Phys*., 1964, **32**, 343.

36 D.-F. Weng, Z.-M. Wang and S. Gao, *Chem. Soc. Rev*., 2011, **40**, 3157.

37 J.-R. Li, Q.Yu, E. C. Sañudo, Y. Tao and X.-H. Bu, *Chem. Commun*., 2007, 2602.

38 T.-T. Wang, M. Ren, S.-S. Bao, B. Liu, L. Pi, Z.-S. Cai, Z.-H. Zheng, Z.-L. Xu and L.-M. Zheng, *Inorg. Chem.,* 2014, **53**, 3117.

39 D. Shao, S.-L. Zhang, X.-H. Zhao and X.-Y. Wang, *Chem. Commun*., 2015, **51**, 4360.

40 M. G. Pini, A. Rettori, L. Bogani, A. Lascialfari, M. Mariani, A. Caneschi and R. Sessoli, *Phys. Rev. B.,* 2011, **84**, 094444.

41 S. M. J. Aubin, Z. Sun, L. Pardi, J. Krzystek, K. Folting, L.-C. Brunel, A. L. Rheingold, G. Christou and D. N. Hendrickson, *Inorg. Chem*., 1999, **38**, 5329.

42 C. Coulon, H. Miyasaka and R. Clerac, *Struct. Bonding*: Berlin, 2006, **122**, 163.

43 J.-Y. Zhang, K. Wang, X.-B. Li and E.-Q. Gao, *Inorg. Chem*., 2014, **53**, 9306.

Table 1 Crystal data and structure refinement for **1** [a]

	1
Chemical formula	$C_{22}H_{20}CoO_7$
F_w	455.31
Cryst size (mm)	0.18 × 0.17 × 0.07
Cryst syst	monoclinic
Space group	*P*2/*c*
a (Å)	19.851(4)
b (Å)	6.3428(13)
c (Å)	8.0146(17)
β (deg)	99.773(3)
V (Å^3)	994.5(4)
Z	2
D_c (g cm^{-3})	1.520
F(000)	470
μ (mm^{-1})	0.906
Reflections collected / unique	4890 / 1753
R_{int}	0.0196
Data / restraints / params	7370 / 1 / 523
R_1 [a], wR_2 [b] ($I > 2\sigma(I)$)	0.0287 / 0.0718
R_1, wR_2 (all data)	0.0326 / 0.0740
Max. and min. transmission	0.9393 and 0.8540
GOF on F^2	1.062
$\Delta\rho_{max}$, $\Delta\rho_{min}$ / e·Å^{-3}	0.286, – 0.229

[a] $R_1 = \Sigma||F_o|-|F_c||/|F_o|$. [b] $wR_2 = [\Sigma w(|F_o^2|-|F_c^2|)^2/\Sigma w(|F_o^2|)^2]^{1/2}$.

Table 2. Selected bond distances (Å) and angles (°) for **1** [a]

Co(1)–O(1)	2.0292(15)	Co(1)–O(3W)	2.0491(17)
Co(1)–O(4W)	2.2297(9)		
O(1)–Co(1)–O(3W)	93.69(9)	$O(1)^{\#1}$–Co(1)–O(3W)	86.31(9)
O(3W)–Co(1)–O(4)	94.09(6)	O(1)–Co(1)–O(4)	93.11(5)
$O(1)–Co(1)–O(4W)^{\#1}$	86.89(5)	$O(3W)–Co(1)–O(4W)^{\#1}$	85.91(6)

[a] Symmetry codes: $^{\#1}$ $1 – x$, $1 – y$, $2 – z$.

Table 3. Hydrogen-bonding parameters (Å, °) for **1** [a]

D–H···A	*d* (D–H)	*d* (H···A)	*d* (D···A)	∠(D–H···A)
O3W–H3A···O1$^{\#1}$	0.850	1.857	2.689	165.98
O3W–H3B···O2$^{\#2}$	0.850	2.032	2.785	147.29
O4–H4A···O2$^{\#3}$	0.850	1.785	2.620	166.90

[a] Symmetry codes: $^{\#1}$ $1-x, -y, 2-z$. $^{\#2}$ $1-x, -y, 2-z$; $^{\#3}$ $1-x, y, 5/2-z$.

Captions to Figures

Fig. 1 1D chains of **1** (top) and **2** (bottom) extended by bridging water molecules (Hydrogen atoms were omitted for clarity, symmetry codes: A = 1 – *x*, 1 – *y*, 2 – *z*; B = 1.5 – *x*, 0.5 + *y*, 0.5 – *z*).

Fig. 2 2D network of **1** (top) and **2** (bottom) generated by interchain hydrogen-bonding and/or C–H···π interactions.

Fig. 3 Temperature dependence of $\chi_M T$ for **1** (left) and **2** (right) at 1 kOe (Solid lines represent the best fits indicated in the text. Inset: Field-cooled χ_M curves at different fields).

Fig. 4 Isothermal magnetizations for **1** and **2** measured at 2.0 K. Inset: magnetic hysteresis loops for **1** and **2** measured at selected temperatures.

Fig. 5 Magnetic (*T*, *H*) phase diagram for **1** constructed from variable-field (●) and variable-temperature (×) magnetic susceptibility data.

Fig. 6 Temperature dependence of ac susceptibilities for **2** at the selected frequencies under H_{ac} = 3.5 Oe and H_{dc} = 0 Oe (Inset: Arrhenius plot of relaxation rate as a function of reciprocal temperature).

Fig. 7 ln($\chi'T$) versus 1/*T* plot for **2** at 1 Hz under H_{dc} = 0 Oe and H_{ac} = 3.5 Oe. The solid line represents the best fit to a 1D Ising model.

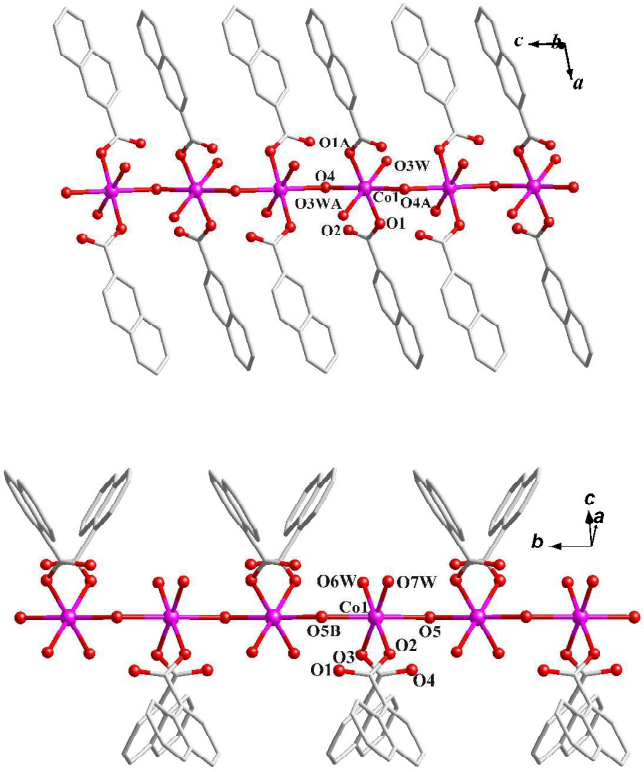

Fig. 1

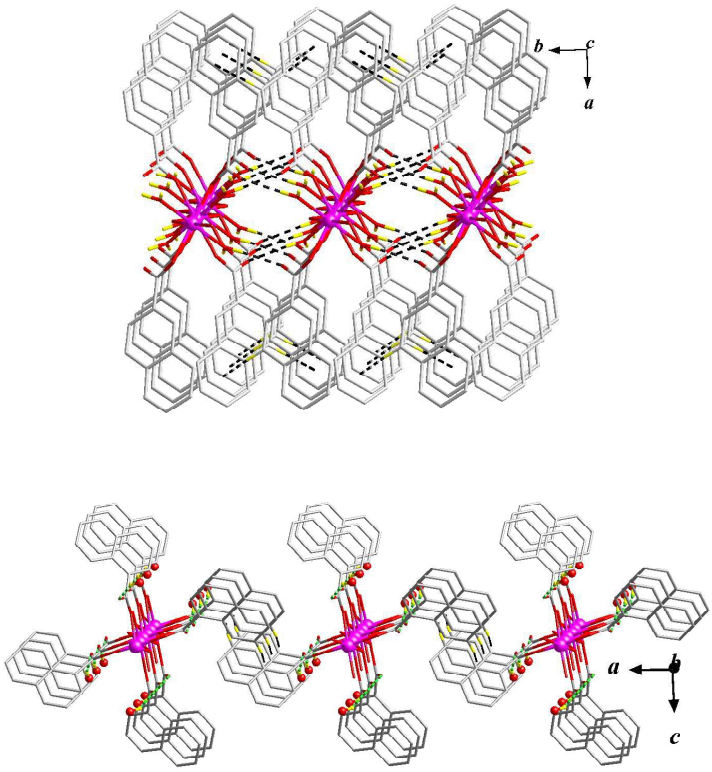

Fig. 2

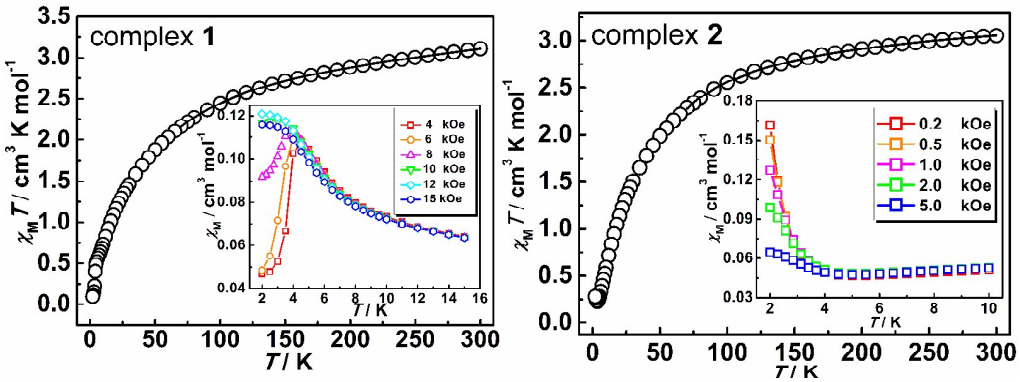

Fig. 3

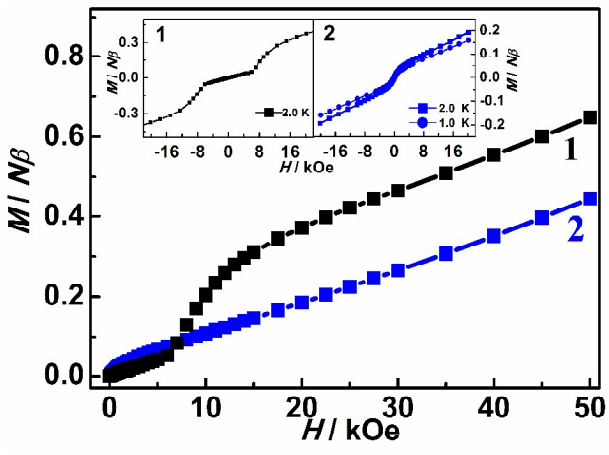

Fig. 4

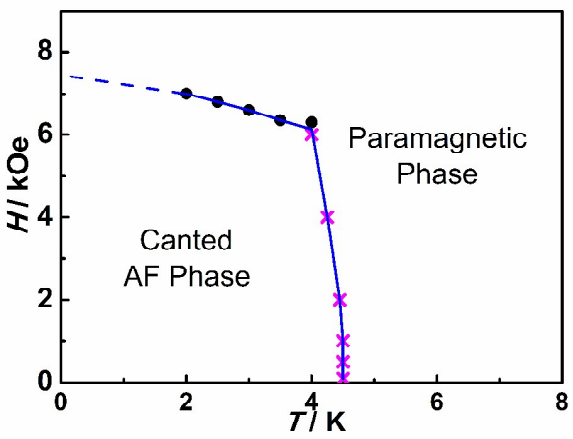

Fig. 5

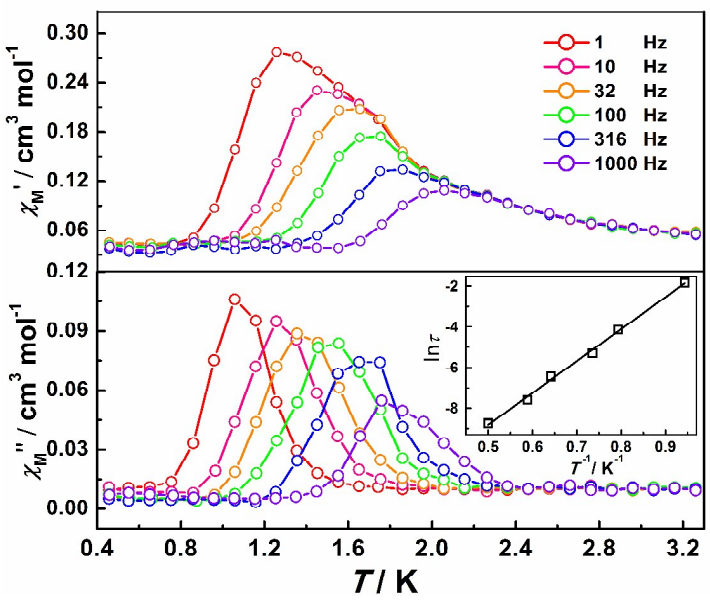

Fig. 6

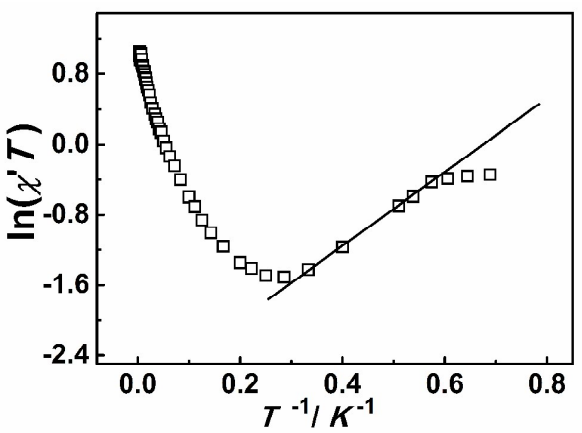

Fig. 7

Graphic Abstract

Two water-bridged cobalt(II) chains with isomeric naphthoate spacers: from metamagnetic to single-chain magnetic behaviour

Zhong-Yi Liu,[a] Yan-Fei Xia,[a] En-Cui Yang,[a,*] and Xiao-Jun Zhao [a,b*]

Two water-bridged cobalt(II) chains with isomeric naphthoate spacers exhibit metamagnetic and SCM behaviours, arising from the dramatically different interchain stacking induced by naphthoate isomers.